Supplementary Information

Remarkable Surface Enhanced Raman Scattering on Self-assembled {201} Anatase

Yaqin Yu, [†,‡] *Jingjing Du,* [†,‡] *and Chuanyong Jing* [*,†,‡]

[†]State Key Laboratory of Environmental Chemistry and Ecotoxicology, Research Center for Eco-Environmental Sciences, Chinese Academy of Sciences, Beijing 100085, China.

[‡]University of Chinese Academy of Sciences, Beijing 100049, China.

Corresponding Author

*E-mail: cyjing@rcees.ac.cn

1. Chemicals and Materials.

N, N dimethyl formamide (DMF), tetrabutyltitanate (TBOT), P25, and dopamine (DA) were purchased from Sigma-Aldrich (St. Louis, US). Hydrofluoric acid (HF), sodium hydroxide (NaOH), potassium hydroxide (KOH), and sodium chloride (NaCl) were from Sinopharm Chemical Reagent Co., Ltd (China). Mili-Q water (>18.2 MΩ) was used to prepare all the solutions.

2. Fabrication of Faceted TiO_2 Nanocrystals.

{201} TiO_2: 8 mL HAc and 12 mL DMF were mixed under magnetic stirring, and 0.5 mL tetrabutyltitanate (TBOT) was added dropwise. After reacting for 10 min at room temperature, the homogeneous solution was transferred into a 100 mL Teflon-lined stainless-steel autoclave and kept in an electric oven at 180 ^{o}C for 12 h. After cooled down, the precipitate was separated by centrifugation at 10000 rpm for 10 min, washed with ethanol for five times, and then oven dried at 60 ^{o}C overnight.[1]

{001} TiO_2: 2.5 mL TBOT was added to 60 mL isopropyl alcohol. After the solution was gently stirred for a few minutes, 1 mL HF was added dropwise. The solution was then transferred to a 100 mL autoclave and kept in oven at 200 ^{o}C for 24 h. After cooled to room temperature, the resulted precipitate was harvested via centrifugation, washed thoroughly with ethanol, and dried at 60 °C overnight.[2]

{101} TiO_2: 2 g P25 was added to 80 mL of 10 mol·L^{-1} KOH solution under magnetic stirring to form a white suspension. The suspension was equally divided into two 100 mL autoclaves and kept at 200 ^{o}C for 24 h. The resulted precipitate was washed with HCl for several times to attain pH=5, then finally dried at 60°C overnight. After that, 0.2 g of the prepared potassium titanate nanowires (KTNWs) were dispersed in 24 mL deionized (DI) water under ultrasonic treatment for 1 h. The solution was then transferred into a 100 mL autoclave and kept at 200 ^{o}C for 48 h. The products were collected by centrifugation at 10000 rpm for 10 min, washed with DI water and oven dried at 60 ^{o}C overnight. [3]

48 {100} TiO_2: 2 g P25 was added to 80 mL of 10 mol·L^{-1} NaOH solution under magnetic
49 stirring to form a white suspension. The suspension was then transferred to a 100 mL autoclave
50 and kept in oven at 120 ^oC for 24 h. Sodium titanate nanowires (NaTNWs) were separated from
51 solution by centrifugation and washed with DI water to attain pH=10.5. After that, 2 g NaTNWs
52 were dispersed into 80 mL DI water, then transferred to a 100 mL autoclave and heated at 200
53 ^oC for 24 h. The resulted white precipitates were separated from solution by centrifugation,
54 washed with DI water, and finally oven dried at 60 ^oC. [4]

55 **3. Characterizations.**

56 The surface morphology of TiO_2 was examined using a field emission scanning electron
57 microscope (FE-SEM, SU-8000, Hitachi, JPN) and high resolution-transmission electron
58 microscope (HRTEM, JEM-2100F, JEOL. Ltd., JPN) The crystal structure was determined
59 using an X'Pet PRO diffractometer (PANalytical, Netherlands) with Cu Kα radiation.
60 The Brunauer-Emmet-Teller (BET) specific surface area was recorded form N_2 adsorption-
61 desorption isotherms using a Surface Area and Porosity Analyzer (ASAP 2020 Plus HD88,
62 Micromeritics, USA) after degassed in a vacuum at 120^oC for 12 h. The electron
63 paramagnetic resonance (EPR) signals were recorded on a Bruker EMX plus
64 spectrometer (LOT-Oriel Gmbh&Co. KG, Germany). The surface OH density was detected
65 based on thermogravimetric analysis (TGA) using a TA SDTQ600 (TA instruments, USA). The
66 UV-vis diffuse reflectance spectra (DRS) were recorded on a scanning UV-vis
67 spectrophotometer (UV-DRS, UV-2450, Shimadzu, JPN) equipped with an integrating sphere
68 assembly, while $BaSO_4$ was used as a reference.

69 **3.1. SEM and TEM.**

70 The SEM and TEM images (**Figure 1**A1, B1) show that {201} TiO_2 crystals were sea urchin-
71 like spheres (radius = 500 nm) with exposed {201} facets and unexposed {401} facets.[1] The
72 {100} TiO_2 nanorods about 500 nm in length exposed dominant {100} facets (80%) with a
73 lattice spacing of 0.38 nm (Figure 1A2, B2).[4] The highly truncated bipyramidal {001} TiO_2

exhibited two square {001} facets (82%) with a lattice spacing of 0.19 nm.[2] The thickness of {001} TiO_2 is 6 nm and a length of 40-50 nm (Figure 1A3, B3). The {101} TiO_2 was octahedral crystal with the long axis size of 100 nm (Figure 1A4, B4), and the measured lattice spacing was 0.35 nm corresponding to the {101} facet (98%).[3]

3.2. XRD Spectra.

The powder X-ray diffraction (XRD) spectra (**Figure S1**) illustrated that the crystal phase of four samples was anatase ($I4_1$/amd, No. 01-084-1286). The tetragonal unit cell of anatase grows preferentially along the [101] orientation, resulting in highest (101) diffraction peak in XRD spectra.

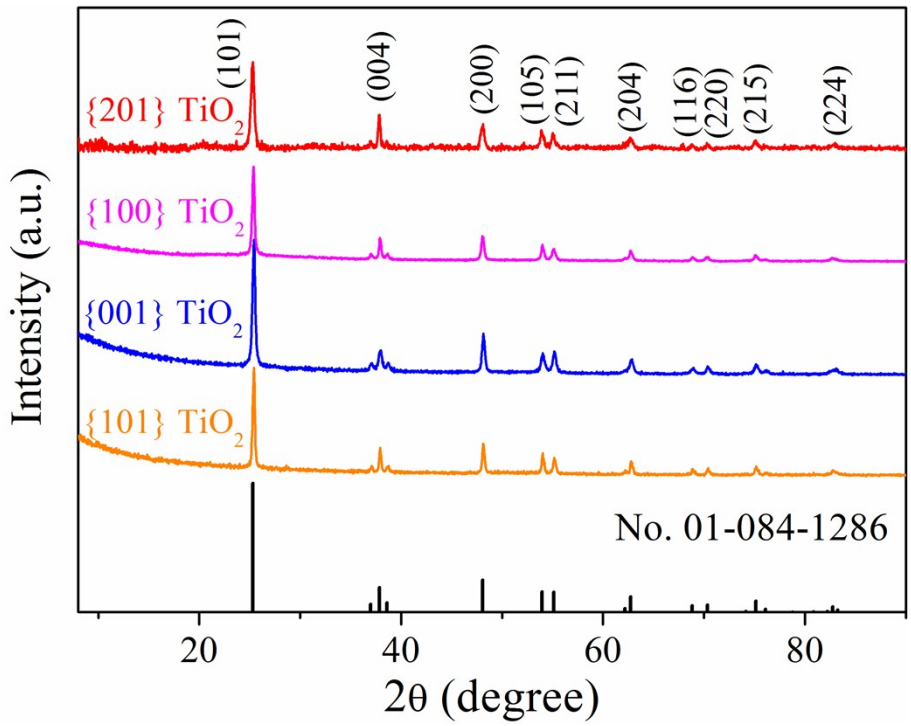

Figure S1. XRD characterization of TiO_2 with {101}, {100}, {001}, and {201} facets.

3.3. Physicochemical Properties of Four Facets.

The differences in morphology of four facets contributed to the various specific surface area (S_{BET}), {101} (23.49 $m^2 \cdot g^{-1}$) > {201} (23.22 $m^2 \cdot g^{-1}$)> {001} (21.17 $m^2 \cdot g^{-1}$) > {100} (16.54

$m^2 \cdot g^{-1}$). The concentration of oxygen vacancy (g=2.00013) followed the order {100} > {201} > {101} > {001} (**Figure S2**A1-A4), contributed to the specific atomic structure. The surface OH density of {201}, {100}, {001}, and {101} TiO_2 was 3.6, 3.8, 6.7, and 0.9 $OH \cdot nm^{-2}$ (Figure S2B1-B4), ascribed to the different under-coordinated Ti sites. The crystal plane has a great impact not only on TiO_2 morphology and surface atomic arrangement, but also on its physical and chemical properties.

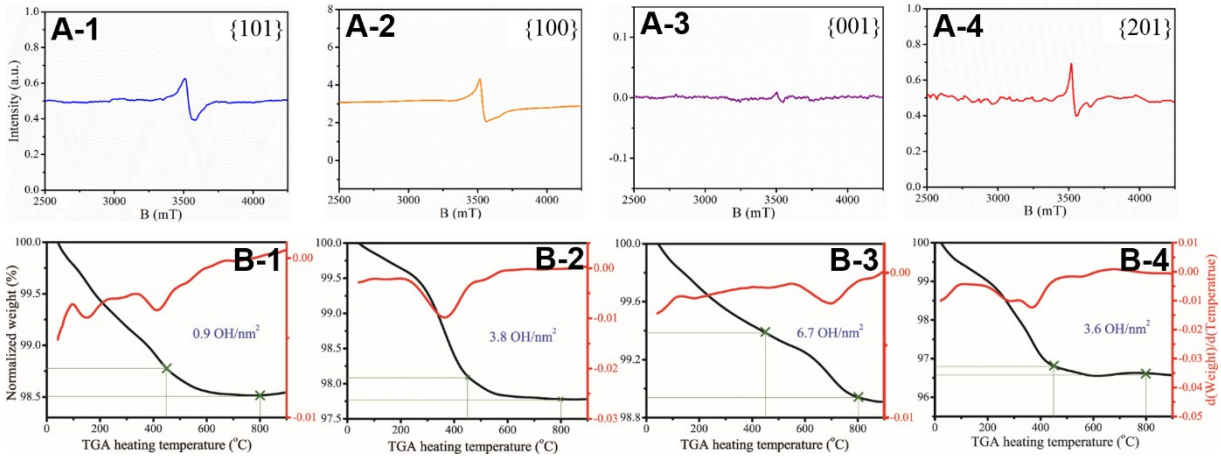

Figure S2. EPR spectra (A1-A4) and TGA curves (B1-B4) of TiO_2 with {101}, {100}, {001}, and {201} facets.

4. SERS Experiments.

Dopamine (DA) was employed as the probe molecule. A mixture containing 10^{-4} to 10^{-6} M DA and 0.1 $g \cdot L^{-1}$ TiO_2 was dropped on silicon wafers and detected by the state translation nanoparticle-enhanced Raman spectroscopy (STNERS) method, which is based on transition from wet to dry states. [5] Raman spectra were collected on a laser confocal microscopy Raman spectrometer (LabRAM HR Evolution, HORIBA, JPN) with excitation wavelength at 532 nm. The spectra were acquired for 10 s with three accumulations. For each sample, the final Raman spectrum was an average of fifteen Raman spectra at different positions on the sample. The rough first-order enhancement factors (EFs) was approximately estimated by comparing intensity of primary peak at 1484 cm^{-1} according to the following equation (1)

$$EF = (I_{SERS}/I_R) \times (N_R/N_{SERS}) \quad (1)$$
$$N_R = (C_R \times V_R)/S_R \quad (2)$$
$$N_{SERS} = (C_{SERS} \times V_{SERS})/S_{SERS} \quad (3)$$

where I_{SERS} and I_R are the intensity of same Raman band for SERS and non-SERS spectra of DA, respectively, and N_{SERS} and N_R are the average number of DA molecules in scattering area for SERS and non-SERS measurement. C_R and C_{SERS} are the molar concentration of DA without and with TiO_2 substrate, V_R and V_{SERS} are the volume of DA droplet. S_{SERS} is the effective area of TiO_2 substrate after solvent evaporation, S_R is the area of DA droplet on Si wafers after evaporation.

Table S1. SERS-active TiO_2 semiconductors

Semiconductors	Analyte	Maximum EF	Excited wavelength (nm)	Ref.
TiO_2 particle	pyridine	low	514.5	6
TiO_2 mesoporous film	N719 dye	Low	532	7
TiO_2 particle	4-MBA	10^2-10^3	514.5	8-9
TiO_2 NPs	dopamine	10^3	442	10-11
TiO_2 colloid	pyrocatechol		514.5	12
TiO_2 NPs	nitrothiophenol	10^2-10^3	633	13
3D nanostructure	dye	10^6	532	14
TiO_2 microarray	MB	10^4	532	15
TiO_2 electrode	cytochrome b5	8.6	413	16
Mesoporous TiO_2 NPs	4-MBA	10^3-10^5	532	17-18
TiO_2, WO_3 film	R6G	10^3-10^5	532	19-20
$W_{18}O_{49}$	R6G	3.4×10^5	532.8	21
Cu_2O	R6G	8.0×10^5	647	22
Cu_2O concave sphere	crystal violet	2.8×10^5	647, 514.5	23
{201} TiO_2	dopamine	1.6×10^6	532	**This work**

Table S2. Raman frequency (cm^{-1}) and assignment of DA.

Band	DA	{201}-DA	{100}-DA	{001}-DA	{101}-DA	Assignment
ν_{15}	1150	1156	1152	1152	1152	N-H in-plane vibration[24]
ν_{C-O}	1289	1268	1272	1272	1274	Stretching vibrations of the catechol carbon−oxygen[25]
ν_3	1324	1334	1335	1335	1335	Bending vibrations of the aromatic carbon−hydrogen, ν (C-H)[25]
ν_{19a}	1466	1426	1432	1434	1432	Stretching vibration of the C-C[24]
ν_{19b}	1528	1484	1491	1494	1491	Stretching vibration of the C-C bond attached with oxygen[25]

Figure S3 shows Raman spectra of DA with 5×10^{-4}, 5×10^{-5} to 5×10^{-6} M concentrations. The selective enhancement indicates that the SERS behavior of {201} TiO_2 largely depends on different coordination environment. [21]

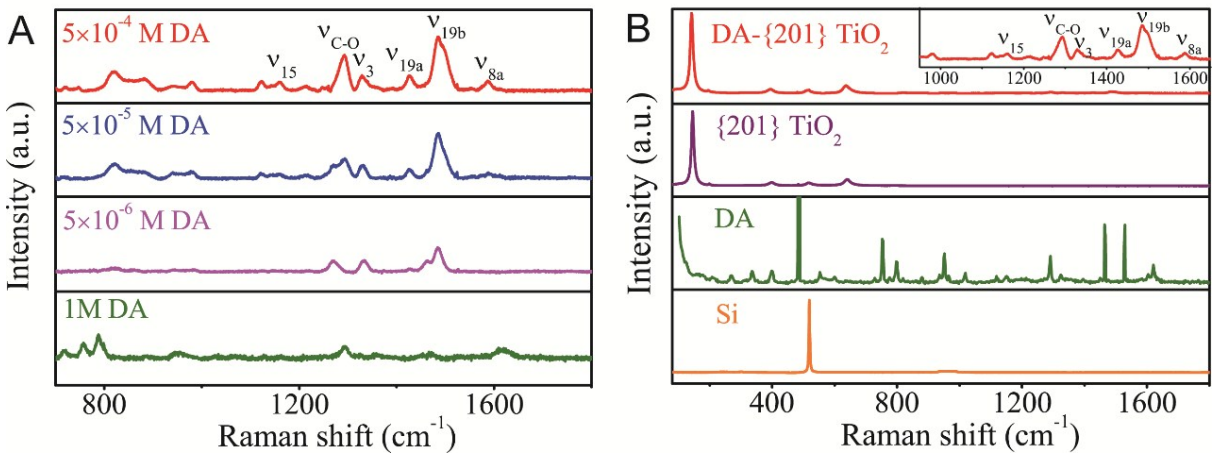

Figure S3. (A) Raman spectra collected for {201} TiO_2 at three different concentrations DA (5×10^{-4}, 5×10^{-5}, and 5×10^{-6} M). (B) Raman profile of DA (5×10^{-4} M) on substrates deposited with {201} TiO_2 sample compared with that for bare Si and {201} TiO_2 substrate.

5. Online *In Situ* Flow Cell ATR-FTIR.

Flow-cell attenuated total reflectance (ATR) Fourier transform infrared (FTIR) experiments were performed using a Thermo-Nicolet iS50R FTIR spectrometer equipped with a liquid-nitrogen cooled MCT detector. The FTIR information was summarized in **Table S3**, and the peak assignments were conducted based on literature. [25] Compared with DA standard (**Figure S4**), phenol hydroxyl bending vibration ν (C-OH) at 1206 cm^{-1} was absent, and Ti-O-C stretching vibration at 1226 cm^{-1} was present in the spectrum of {201} TiO_2-DA. The occurrence was associated with the chemical bonding of DA to {201} TiO_2 following a double deprotonation and forming two O-Ti bonds with two surface under-coordinated Ti sties.

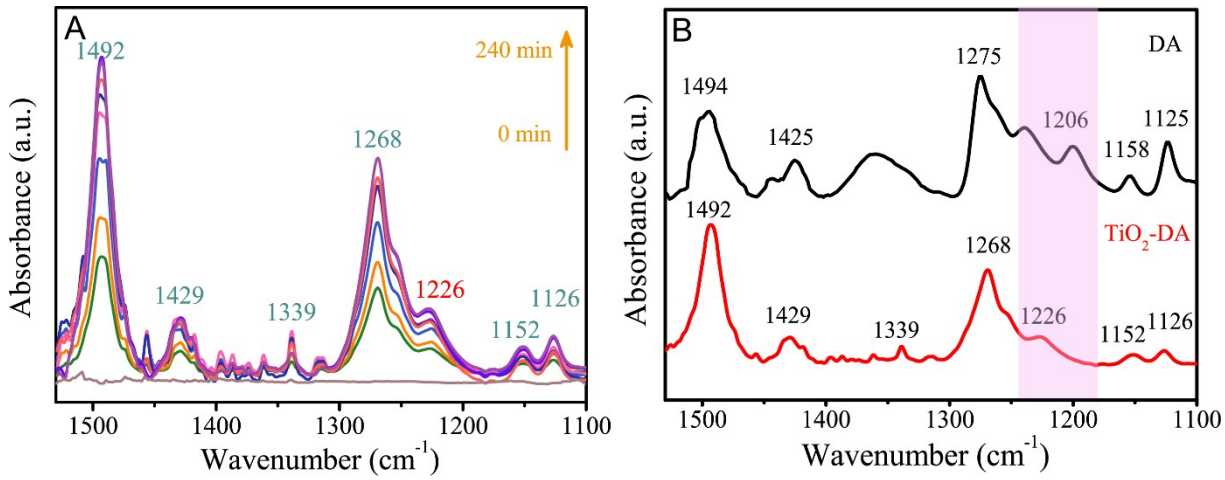

Figure S4. (A) *In situ* ATR-FTIR spectra for DA adhesion to {201} TiO_2 at pH 5. (B) FTIR spectra for DA and {201} TiO_2–DA.

Table S3. FT-IR frequency (cm^{-1}) and assignment of DA.

Peak position / cm^{-1}	Assignment
1125	C-C stretching vibration
1158	C-C stretching vibration
1206	in-plane bending vibrations of the phenolic group C-OH
1275	CH_2 bending vibrations
1425	δ(N-H)
1494	aromatic C=C stretching vibration

6. DFT Calculations.

Density functional theory (DFT) calculations were performed using Castep package in Materials Studio 7.0 (Accelrys, San Diego, CA). The slab model was cleaved, five layers of atoms were extracted, and a 2×2 supercell was built with a vacuum slab of 15 Å. A plane-wave cutoff energy of 340 eV was selected, and ultrasoft pseudopotentials were used in the treatment of core electrons. The exchange-correlation energy was calculated with the generalized gradient approximation (GGA) mode of Perdew-Burke-Ernzerhof (PBE). The k-point over the Brillouin zone was set as a 1×2×1 grid. The BFGS method was employed for geometry optimization until the SCF and energy tolerances were less than the convergence criteria. The DFT+U method was employed, and U=4.0 eV was used, as determined previously. [26]

The adsorption energies (E_{ads}) was calculated according to the equation:

$$E_{ads}=E_{mol+surf} - (E_{surf} + E_{mol}) \quad (4)$$

Where $E_{mol+surf}$ is the total energy of surface complexes; E_{surf} is the energy of isolated TiO_2 facets; and E_{mol} is the energy of an isolated DA molecule. Note that a negative value for E_{ads} suggests a stable adsorption configuration.

To investigate the change of electron density upon adsorption, the electron density difference (Δρ) was calculated by subtracting the electron density of the isolated DA ($\Delta\rho_{DA}$)

and surface ($\Delta\rho_{surf}$) from the total electron density of the system ($\Delta\rho_{DA+surf}$) as follows: $\Delta\rho = \Delta\rho_{DA+surf} - (\Delta\rho_{surf} + \Delta\rho_{DA})$.

6.1. Adsorption Mode of DA on {201} TiO_2.

Multiple possibilities of DA adsorption on {201} TiO_2 surface were considered (**Figure S5**). The bidentate mode of OH groups of DA bonding on two under-coordinated Ti_{4c} sites was the most stable mode based on the adsorption energy.

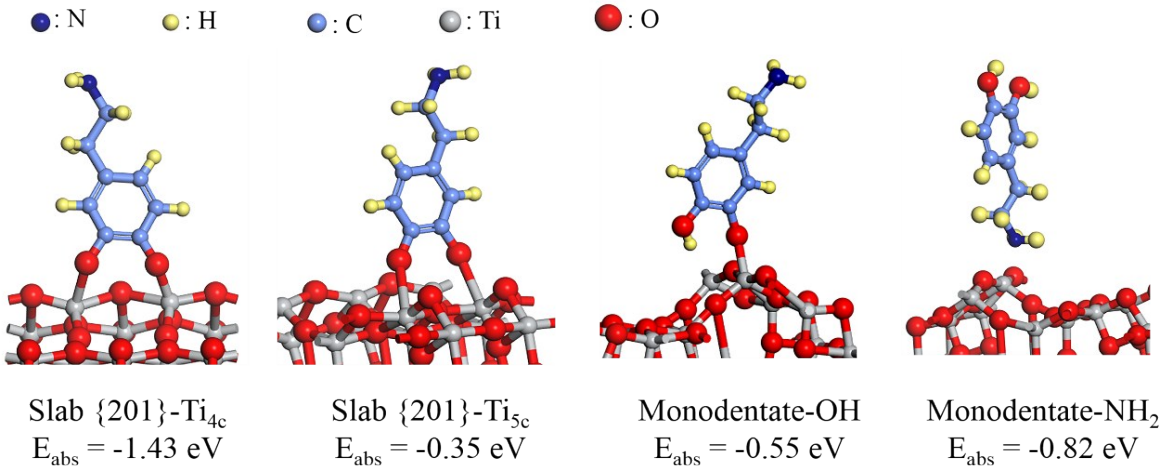

Figure S5. Multiple adsorption mode of DA on the {201} anatase terminations.

6.2. Surface-Active Sites of Four Faceted TiO_2.

The adsorption structure of DA on four facets was the bidentate mode of bonding OH on two under-coordinated Ti sites (**Figure S6**). The active adsorption sites on {101}, {001} and {100} facets are five-coordinated Ti_{5c} atoms, and on {201} facets are four-coordinated Ti_{4c} atoms.

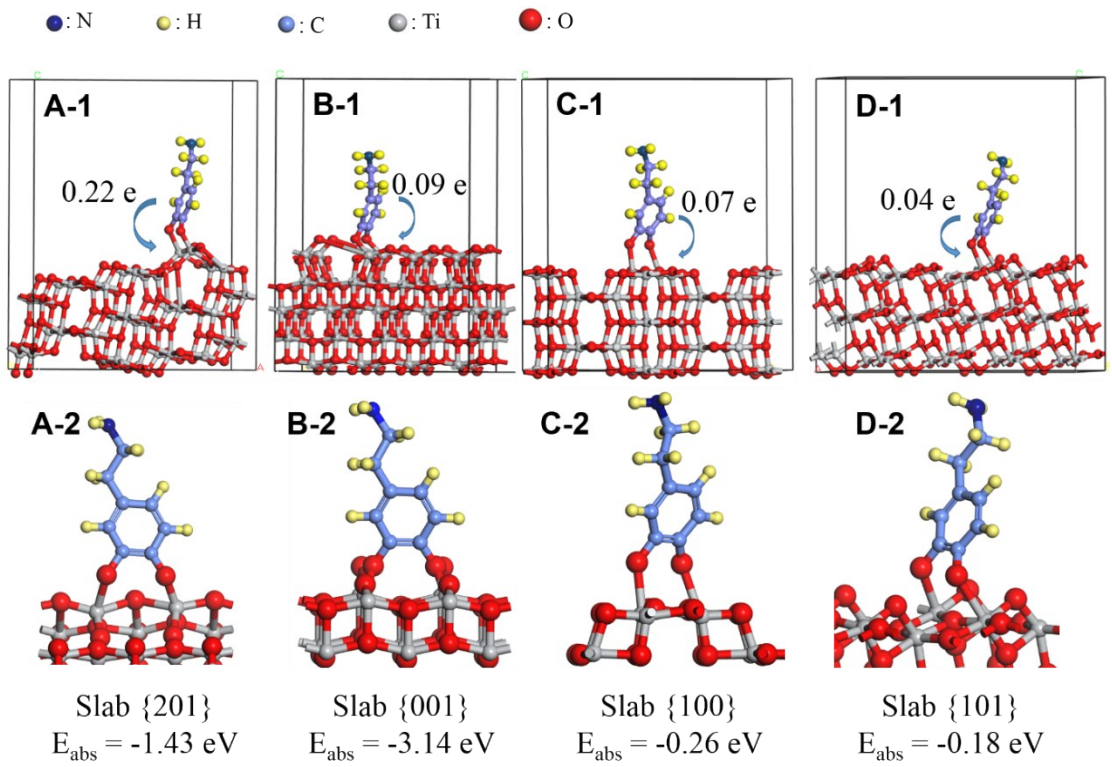

Figure S6. Charge transfer (A-1, B-1, C-1, and D-1) and adsorption energy (A-2, B-2, C-2, and D-2) obtained for {201}, {001}, {100}, and {101} anatase terminations.

6.3 Surface Electronic Structure.

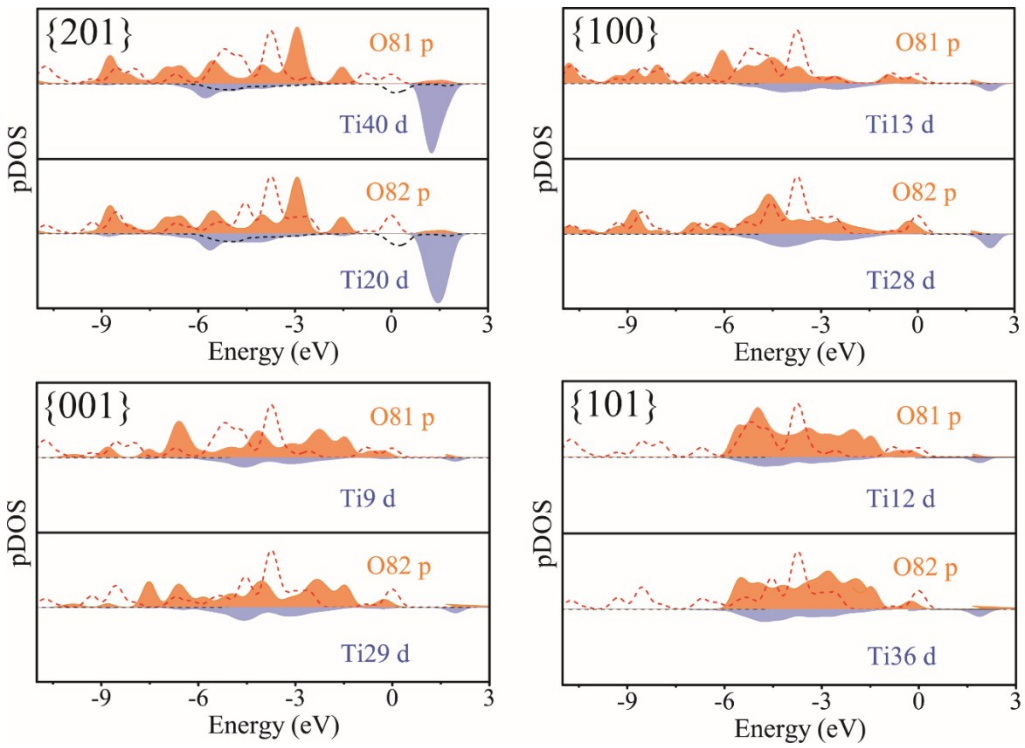

Figure S7. PDOS of O and Ti before (dashed line) and after (solid line with filled area) adsorption for {201} (Ti40 (Ti_{4c}), Ti20 (Ti_{4c}), O81, and O82), {100} (Ti13 (Ti_{5c}), Ti28 (Ti_{5c}), O81, and O82), {001} (Ti9 (Ti_{5c}), Ti29 (Ti_{5c}), O81, and O82), and {101} facets (Ti12 (Ti_{5c}), Ti36 (Ti_{5c}), O81, and O82).

7. Charge Transfer between DA and TiO_2.

7.1. XANES study.

The DA adsorption samples were prepared by reacting 0.1 mM DA with 0.1 $g \cdot L^{-1}$ TiO_2 in 0.01 M NaCl solution at pH 5. After 24 h mixing, the suspensions were centrifuged at 10000 rpm and freeze-dried under vacuum. All solid samples were deposited on one side of a piece of Kapton tape and placed in front of X-ray beam to minimize self-absorption. The K-edge spectra of O and L-edge of Ti were collected at beamline 08U at the Shanghai Synchrotron Radiation Facility (SSRF, China). X-ray absorption near-edge structures (XANES) spectra were acquired from − 20 to 20 eV relative to the O K-edge of 543 eV and the Ti L-edge of 460 eV. Spectral data processing was analyzed using the Athena program in the Demeter computer package.

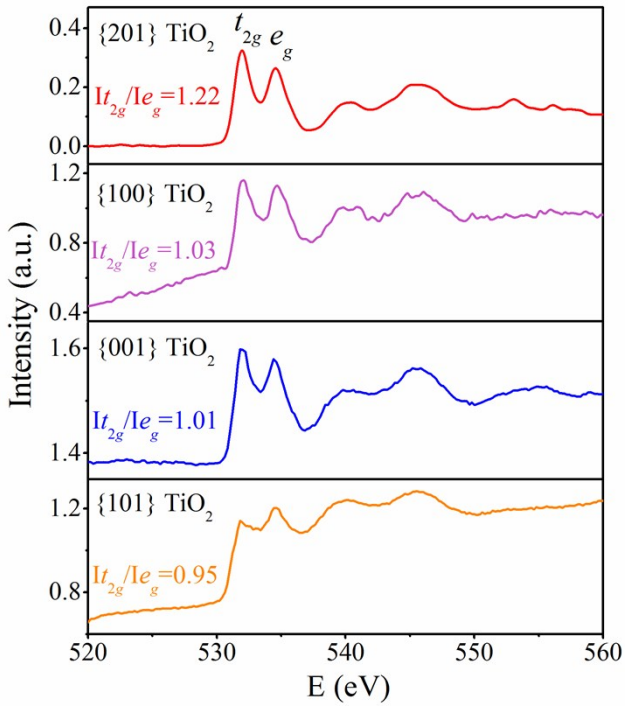

Figure S8. O K-edgeXANES spectra of {201}, {100}, {001}, and {101} TiO_2 samples.

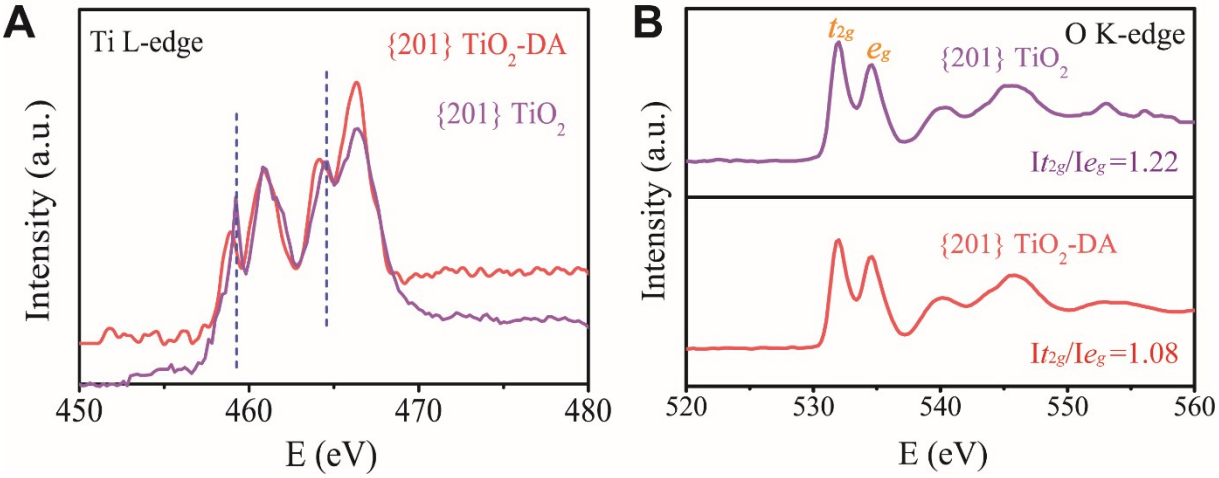

Figure S9. (A) Ti L-edge and (B) O K-edge XANES spectra of DA on {201} TiO_2 samples at pH 5.

Table S4. Intensity of Ti L-edge and O K-edge XANES spectra.

Sample		L_{III}			L_{II}		
		E-t_{2g}	E-e_g	It_{2g}/Ie_g	E-t_{2g}	E-e_g	It_{2g}/Ie_g
TiO_2	Ti L-edge	459.2	460.9	0.90	464.5	466.4	0.87
	O K-edge	531.9	534.5	1.22			
TiO_2-DA	Ti L-edge	458.9	460.8	0.66	464.2	466.3	0.70
	O K-edge	531.9	534.5	1.08			

7.2. UV-DRS Study.

The spectrum for DA-{201} TiO_2 presented increased optical adsorption within the whole visible light range, shifted from the band-band transition for TiO_2 (398 nm) and the photo-absorption onset for DA (312 nm). Interestingly, the absorbance followed the order {201} (0.3) > {100} (0.18) > {001} (0.15) > {101} (0.11) (**Figure S10**).

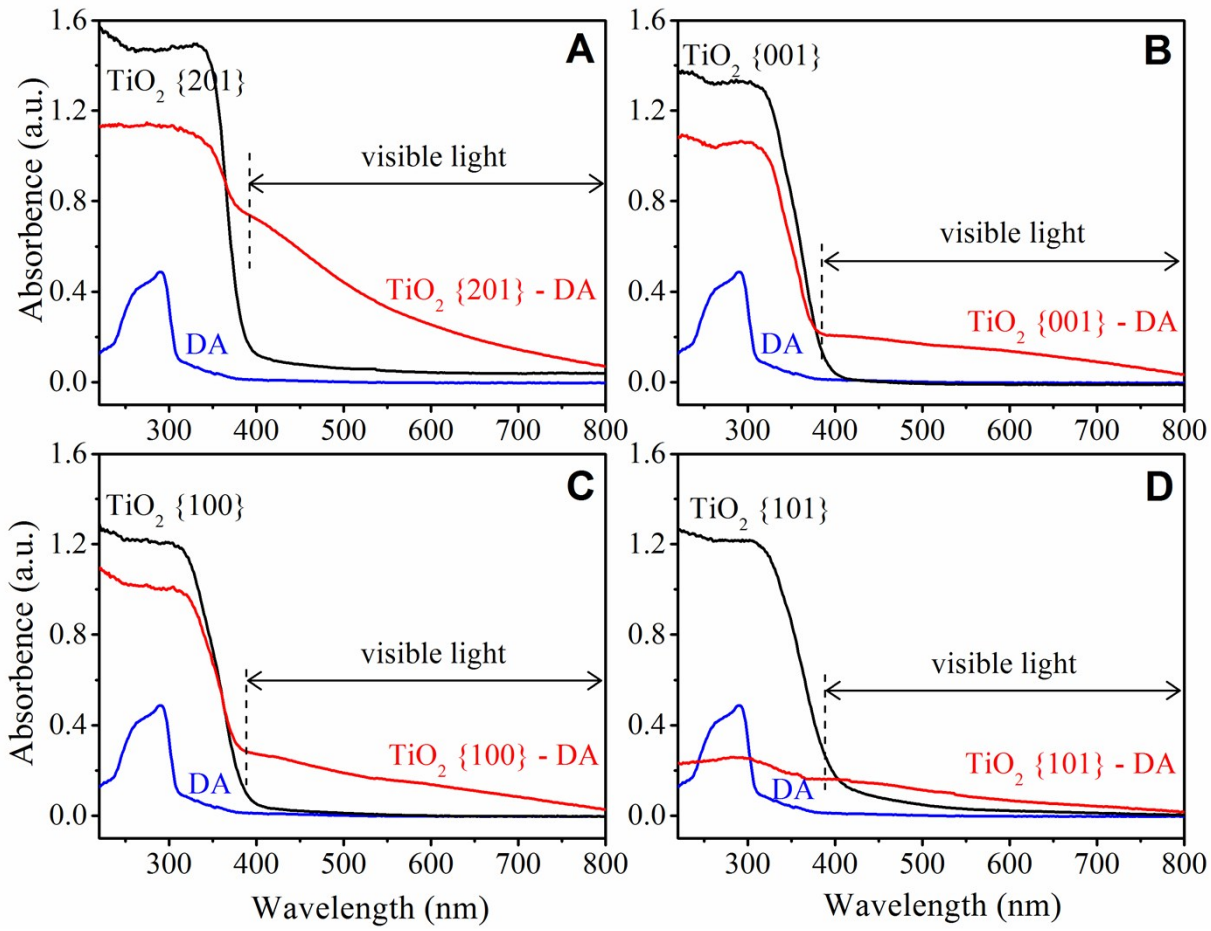

Figure S10. Absorption spectra for DA adsorbed on (A) {201}, (B) {001}, (C) {100}, and (D) {101} TiO_2 compared with neat TiO_2 and DA.

***8. In Situ* Raman-EC Analysis.**

To evaluate the charge transfer between adsorbed DA and TiO_2, *in-situ* Raman-electrochemistry (EC) measurements were performed with a three-electrode system on an electrochemical workstation (PGSTAT302N, Autolab, Switzerland). The commercial glass-carbon electrode (GCE) modified with TiO_2 served as the working electrode, Ag/AgCl as the reference electrode, and Pt wire as the counter electrode. The electrolyte was prepared with 0.1 M NaCl and 0.1 mM DA. The photocurrent responses were measured by chrono-amperometry at an applied potential of 1.23 V under continuous on-off Raman excitation (λ=532 nm) cycles. The difference photocurrent (ΔI) was obtained by subtracting the current without Raman excitation (I_{black}) from the current with Raman excitation (I_{light}) as follow: $\Delta I = I_{light} - I_{black}$.

232

233 **Table S5.** Photocurrent of {201}, {101}, {001}, and {100} TiO_2 electrodes in 0.1 M NaCl

234 without and with 0.1 mM DA.

	Current ($\mu A \cdot cm^{-2}$)	{201} TiO_2	{100} TiO_2	{001} TiO_2	{101} TiO_2
TiO_2	I_{light}	2.36	1.75	2.12	2.18
	I_{dark}	2.28	1.68	2.04	2.10
	ΔI	0.08	0.08	0.08	0.08
TiO_2+DA	I_{light}	24.83	19.03	21.51	21.95
	I_{dark}	23.70	18.14	20.76	21.33
	ΔI	1.13	0.89	0.75	0.63

235

236

237 **Table S6.** Physicochemical properties of four faceted TiO_2.

Facets	E_{sur} (eV)	S_{BET} ($m^2 \cdot g^{-1}$)	OH density ($OH \cdot nm^{-2}$)	Oxygen vacancies (a.u.)	E_{ads} (eV)	It_{2g}/Ie_g	EC current ($\mu A \cdot cm^{-2}$)
{201}	1.72	23.22	3.6	0.7	-1.43	1.22	1.13
{100}	0.89	16.54	3.8	4.42	-0.26	1.03	0.89
{001}	0.75	21.17	6.7	0.01	-3.14	1.01	0.75
{101}	0.63	23.49	0.9	0.63	-0.18	0.95	0.63

238

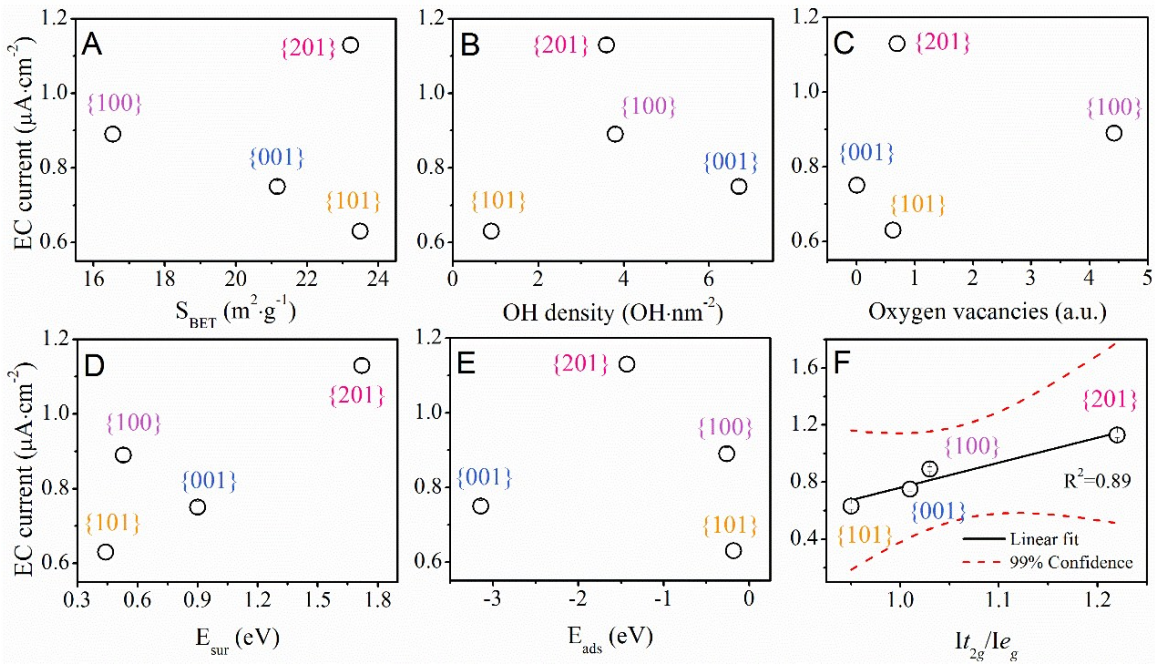

Figure S11. Relationship of EC-measured photocurrent and S_{BET} (A), OH density (B), EPR intensity of oxygen vacancies (C), surface energy (E_{sur}) (D), adsorption energy (E_{ads}) (E), and It_{2g}/Ie_g analyzed by XANES (F).

9. FDTD simulation.

The distribution of electromagnetic field intensity of faceted TiO_2 was simulated with three-dimensional finite difference time domain (FDTD) solutions software (Lumerical Solutions Inc, Vancouver Canada). The mesh size was 1 nm and simulation time was 1000 fs. A 532 nm plane wave light source was used to calculate the electromagnetic field distribution. The refractive index of TiO_2 was 2.55. The light was incident along the z axis, with the polarization along the x axis, and the refractive index of surrounding medium was 1.

Four faceted TiO_2 models were established in accordance with their geometrical parameter determined by SEM and TEM. The {201} TiO_2 spheres (r=500 nm) were composed with exposed {201} facets (α=22.5º) and unexposed {401} facets (α=11.5º). The {100} TiO_2 crystals (l=500 nm) were composed with {100} facets (l=340 nm) and {101} facets (l=80 nm). The {001} TiO_2 particles were truncated bipyramids with side length of 40-50 nm. The {101} TiO_2 particles were octahedral crystals with long axis size of 100 nm.

Considering that asymmetric geometry would impact the transmission of surface plasmon polaritons, the influence of incidence angle (ɵ) on the field distribution was studied in detail by FDTD method.[28-29] For {001} and {100} TiO_2 (**Figure S13 and 14**), as incidence angle increased from 0 º to 90º, the spatial distribution of maximal field enhancement changed from edge to specific face. At the same time, the EF of {001} and {100} TiO_2 decreased from 21 to 9 and from 41 to 15, respectively. Conversely, as incidence angle increased from 0 º to 90º, the EF of {101} and single spline {201} TiO_2 increased from 12 to 136 and from 14 to 50 (**Figure S15 and 16**). The spatial distribution of maximal field enhancement changed from edge to specific face, and then to sharp tips. The different influence of incidence angle on maximal field enhancement indicated that the field enhancement of TiO_2 crystals was influenced by asymmetric structure.

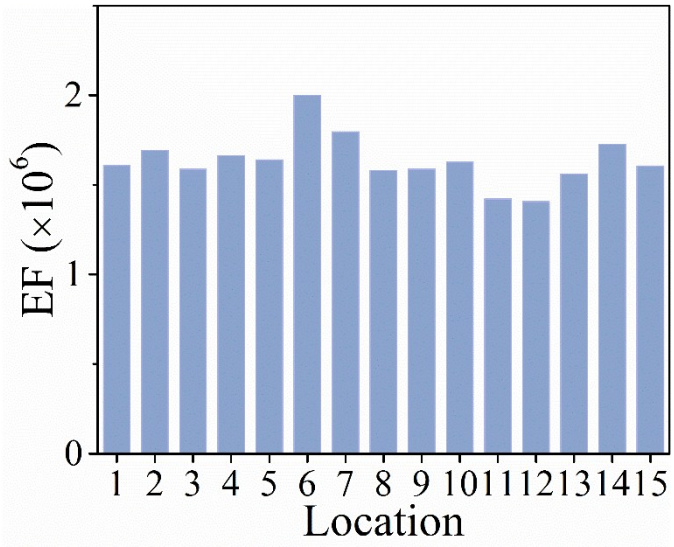

Figure S12. SERS enhancement at 1484 cm^{-1} of fifteen random locations on {201} TiO_2 substrate.

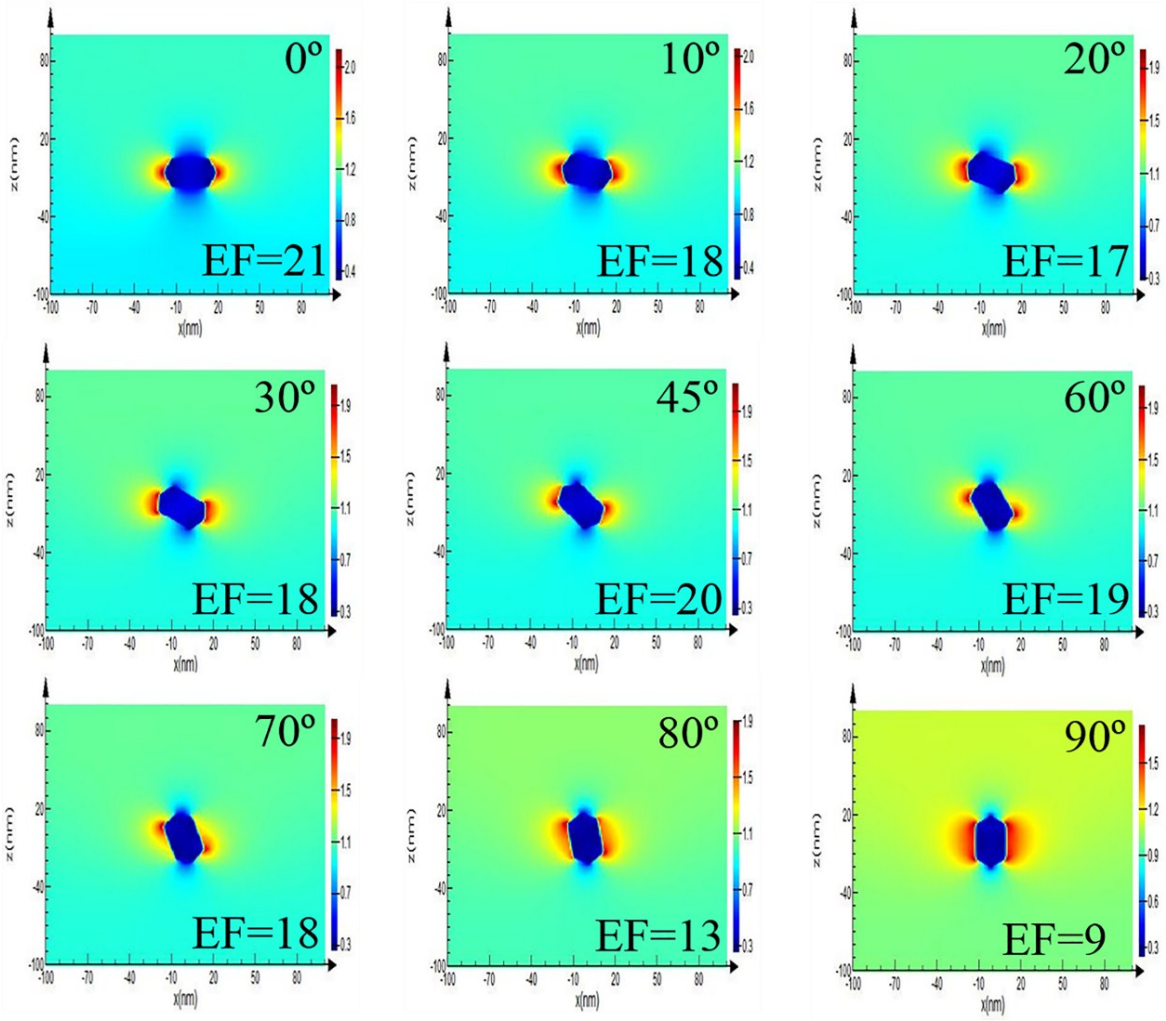

Figure S13. Maximal electric field enhancement of {001} TiO_2 with ɵ=0º, 10º, 20º, 30º, 40º, 50º, 60º, 70º, 80º, 90º.

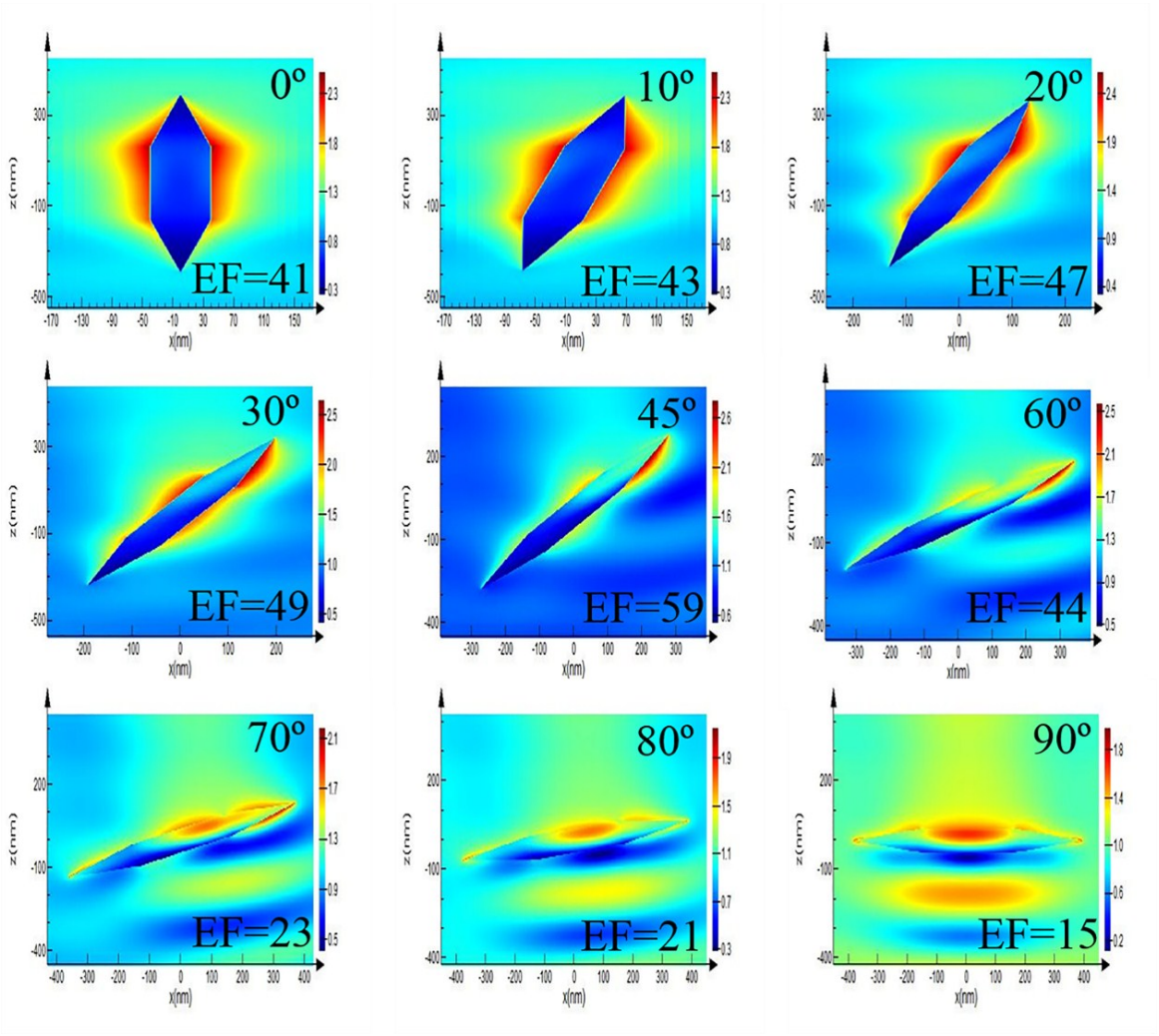

Figure S14. Maximal electric field enhancement of {100} TiO_2 with ɵ=0º, 10º, 20º, 30º, 40º, 50º, 60º, 70º, 80º, 90º.

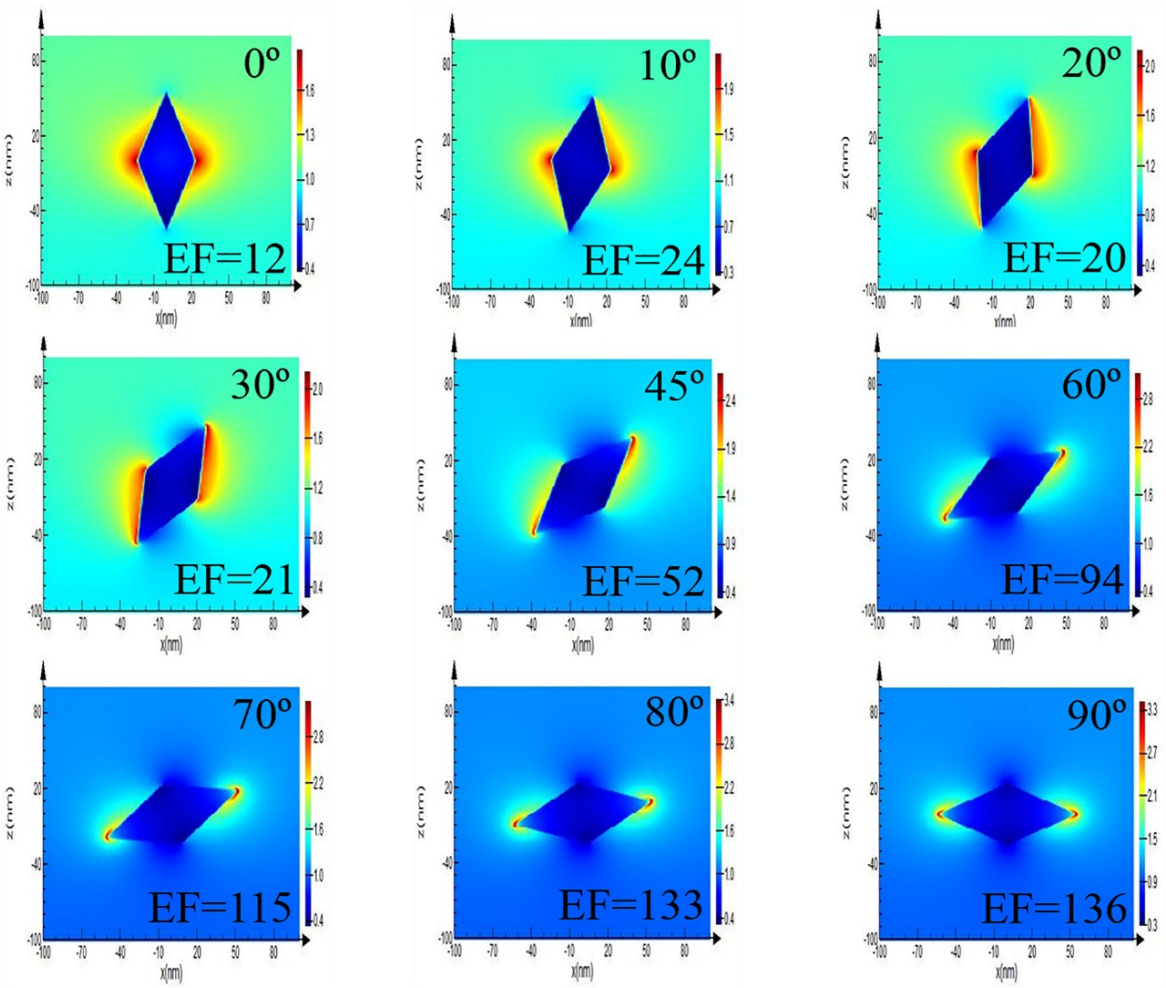

Figure S15. Maximal electric field enhancement of {101} TiO_2 with ɵ=0º, 10º, 20º, 30º, 40º, 50º, 60º, 70º, 80º, 90º.

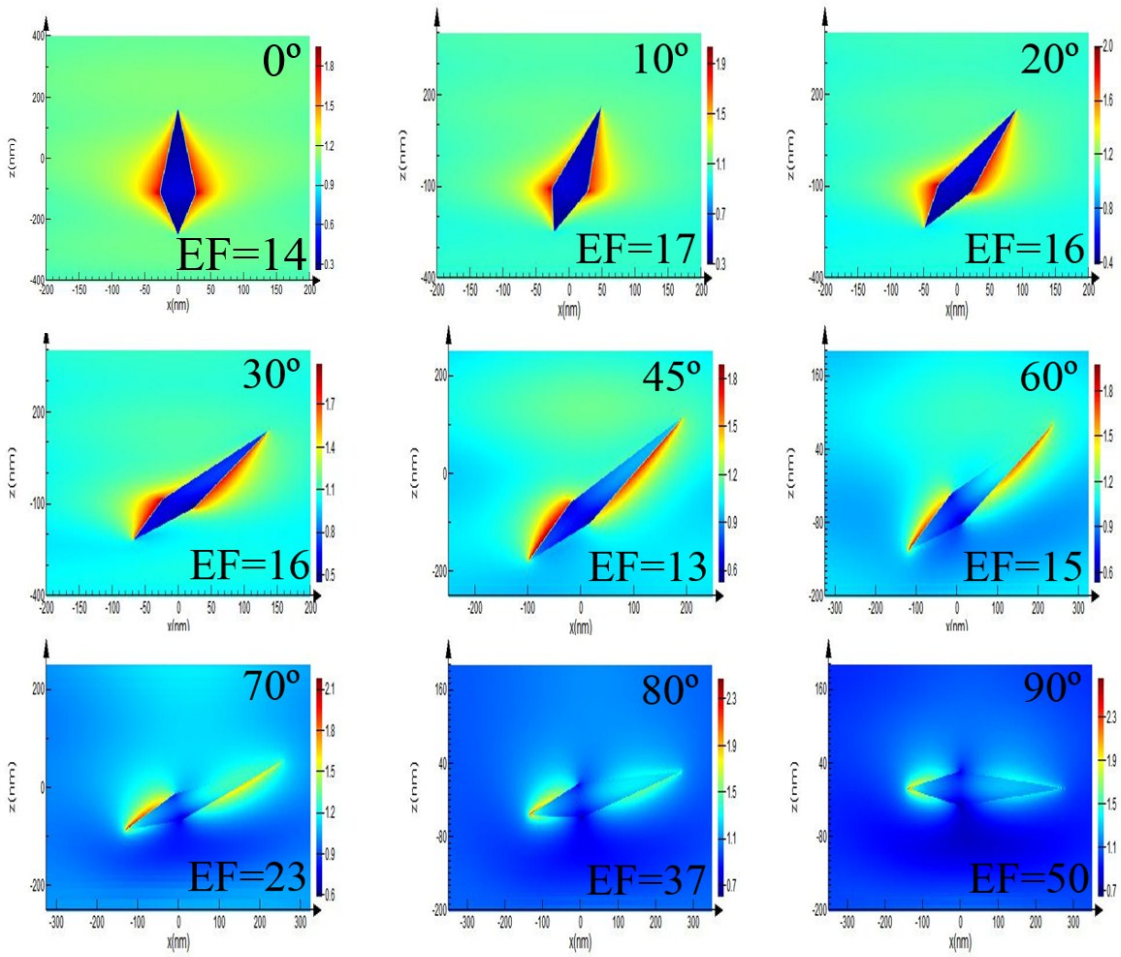

Figure S16. Maximal electric field enhancement of single spine {201} TiO_2 with ɵ=0º, 10º, 20º, 30º, 40º, 50º, 60º, 70º, 80º, 90º.

References

1. H. B. Wu, J. S. Chen, X. W. Lou and H. H. Hng, *Nanoscale*, 2011, **3**, 4082-4084.

2. H. G. Yang, C. H. Sun, S. Z. Qiao, J. Zou, G. Liu, S. C. Smith, H. M. Cheng, and G. Q. Lu, *Nature*, 2008, **453**, 638-641.

3. X. G. Han, F. Zhou, L. Li and C. Wang, *Chem. - Asian J.*, 2013, **8**, 1399-1403.

4. H. T. Gao, X. M. Sui, D. M. Dai, C. D. Si, and G. J. Liu, *J. Nanosci. Nanotechnol.*, 2015, **15**, 5193-5197.

5.L. B. Yang, P. Li, H. L. Liu, X. H. Tang and J. H. Liu, *Chem. Soc. Rev.*, 2015, **44**, 2837-2848.

6. H. Yamada and Y. Yamamoto, *Surf. Sci.*, 1983, **134**, 71-90.

7. C. P. Leon, L. Kador, B. Peng and M. Thelakkat, *J. Phys. Chem. B*, 2006, **110**, 8723-8730.

8. L. Yang, X. Jiang, W. Ruan, B. Zhao, W. Xu and J. R. Lombardi, *J. Phys. Chem. C*, 2008, **112**, 20095-20098.

9. X. Xue, W. Ji, Z. Mao, H. Mao, Y. Wang, X. Wang, W. Ruan, B. Zhao and J. R. Lombardi, *J. Phys. Chem. C*, 2012, **116**, 8792-8797.

10. A. Musumeci, D. Gosztola, T. Schiller, N. M. Dimitrijevic, V. Mujica, D. Martin and T. Rajh, *J. Am. Chem. Soc.*, 2009, **131**, 6040-6041.

11. S. J. Hurst, H. C. Fry, D. J. Gosztola and T. Rajh, *J. Phys. Chem. C*, 2011, **115**, 620-630.

12. W. Ji, W. Song, I. Tanabe, Y. Wang, B. Zhao and Y. Ozaki, *Chem. Commun.*, 2015, **51**, 7641-7644.

13. J. S. Teguh, F. Liu, B. Xing and E. K. L. Yeow, *Chem. - Asian J.*, 2012, **7**, 975-981.

14. D. Maznichenko, K. Venkatakrishnan and B. Tan, *J. Phys. Chem. C*, 2013, **117**, 578-583.

15. D. Qi, L. Lu, L. Wang and J. Zhang, *J. Am. Chem. Soc.*, 2014, **136**, 9886-9889.

16. X. X. Han, C. Koehler, J. Kozuch, U. Kuhlmann, L. Paasche, A. Sivanesan, I. M. Weidinger and P. Hildebrandt, *Small*, 2013, **9**, 4175-4181.

17. L. Yang, D. Yin, Y. Shen, M. Yang, X. Li, X. Han, X. Jiang and B. Zhao, *Phys. Chem. Chem. Phys.*, 2017, **19**, 18731-18738.

18. L. Yang, D. Yin, Y. Shen, M. Yang, X. Li, X. Han, X. Jiang and B. Zhao, *Phys. Chem. Chem. Phys.*, 2017, **19**, 22302-22308.

19. X. Zheng, F. Ren, S. Zhang, X. Zhang, H. Wu, X. Zhang, Z. Xing, W. Qin, Y. Liu and C. Jiang, *ACS Appl. Mater. Interfaces*, 2017, **9**, 14534-14544.

20. M. Wu, H. Wei, Y. Wei, A. Yao, J. Bu, J. Lin, Z. Dong, Y. Chen, Y. Cui and Z. Wu, *Vib. Spectrosc.*, 2018, **95**, 32-37.

21. S. Cong, Y. Yuan, Z. Chen, J. Hou, M. Yang, Y. Su, Y. Zhang, L. Li, Q. Li, F. Geng and Z. Zhao, *Nat. Commun.*, 2015, **6**, 1-7.

22. J. Lin, Y. Shang, X. Li, J. Yu, X. Wang and L. Guo, *Adv. Mater.*, 2017, **29**, 1604797.

23. X. Li, Y. Shang, J. Lin, A. Li, X. Wang, B. Li and L. Guo, *Adv. Funct. Mater.*, 2018, **28**, 1801868.

24. S. Pande, S. Jana, A. K. Sinha, S. Sarkar, M. Basu, M. Pradhan, A. Pal, J. Chowdhury and T. Pal, *J. Phys. Chem. C*, 2009, **113**, 6989-7002.

25. M. L. Roldan, S. A. Centeno and A. Rizzo, *J. Raman Spectrosc.*, 2014, **45**, 1160-1171.

26. I. Urdaneta, A. Keller, O. Atabek, J. L. Palma, D. Finkelstein-Shapiro, P. Tarakeshwar, V. Mujica and M. Calatayud, *J. Phys. Chem. C*, 2014, **118**, 20688-20693.

27. W. Niu, Y. A. A. Chua, W. Zhang, H. Huang and X. Lu, *J. Am. Chem. Soc.*, 2015, **137**, 10460-10463.

28. W. Zhang, Y. Feng, Y. Zhang, W. Chen and W. Lin, *J. Phys. D-Appl. Phys.*, 2015, **48**, 275102.

333 29. B. Liu, Y.-F. Liu, S.-J. Li and X.-D. He, *Opt. Commun.*, 2016, **369**, 44-49.